Numerical Simulation of Case II Transport

Thomas Z. Fu and Christopher J. Durning
Dept. of Chemical Engineering & Applied Chemistry, Columbia University, New York, NY 10025

A nonlinear conservation equation for the fluid concentration field during one-dimensional viscoelastic diffusion is derived by retaining the concentration dependencies of physical properties in the fluid flux expression from the nonequilibrium thermodynamic treatment of Durning and Tabor (1986). The result is specialized to the limit of small, but finite, diffusion Deborah numbers to give a model essentially the same as that by Thomas and Windle (1982) for Case II transport (TW model). Orthogonal collocation on Hermite cubic trial functions together with a stiff ordinary differential equations integrator were used to solve the TW model for integral sorption in a dry film. The solutions show good agreement with previous analyses and confirm that strong nonlinearities in both the fluid diffusivity and the mixture viscosity are essential for prediction from the model of wave-like concentration profiles associated with the Case II process. Also, the numerical results partially confirm the analytical asymptotic analysis of Hui et al. (1987b) for the Case II wave-front velocity, v. They show that Hui et al.'s formula for the dependence of v on characteristic physical properties does not depend on the details of how the diffusivity and viscosity change with fluid content, as long as both are strongly nonlinear.

Introduction

An understanding of unsteady diffusion of low molecular weight fluids in polymers is important in many areas of modern technology. For example, fluid diffusion in polymers plays an important role in photoresist technology (Thompson et al., 1983), in control release technologies (Roseman and Mansdorf, 1983) and in coatings, fiber-spinning and polymer devolatilization operations (Vrentas et al., 1975). It is well known that at temperatures far above the glass transition temperature, the unsteady diffusion follows Fick's law (Fujita, 1968; Crank, 1975). However, near or below the glass transition, the transport often deviates markedly from Fick's law (Park, 1968) and is termed viscoelastic or non-Fickian. Roughly speaking, near the glass transition, the polymer's intrinsic time-dependent response to external disturbance interferes with diffusion and causes deviations from the classical, Fickian transport.

At present, there is no widely accepted, first-principles description of viscoelastic diffusion. There are a number of phenomenological models (see, for example, Astarita and Sarti, 1978; Thomas and Windle, 1982; Petropoulos, 1984; Ocone and Astarita, 1987), but each is based on ad hoc arguments and is limited in the range of conditions that it can handle. A number of first-principles developments based on nonequilibrium thermodynamics have been published (Neogi, 1983; Durning and Tabor, 1986; Carbonell and Sarti, 1990; Jou et al., 1991; Perez-Guerrero and Garcia-Colin, 1991; Edwards and Beris, 1991; Lustig et al., 1992), but none have been systematically tested against reliable data over a broad range of conditions. These circumstances have not permitted adequate modeling of engineering applications involving viscoelastic diffusion. In this article we offer two contributions facilitating such applications.

Firstly, we rederive the one-dimensional (1-D) model of Thomas and Windle (1982) from the results of the nonequilibrium thermodynamic treatment of Durning and Tabor (1986). The development clarifies the empiricism in the original derivation and shows Thomas and Windle's model (TW model) to be a small Deborah number limit of a more general theory of viscoelastic diffusion. Secondly, we present an accurate numerical integration of the TW model, which is known to predict the difficult limit of Case II transport. The numerical techniques that we use for this purpose should be useful for field equations describing viscoelastic diffusion near the Case II limit.

Correspondence concerning this article should be addressed to C. J. Durning.
Current address of T. Z. Fu: International Paper Co., Corporate Research Center, Tuxedo, NY 10987.

This article is organized as follows. The next section summarizes the important phenomenological background on viscoelastic diffusion and the Case II limit. Then we present a new derivation of the TW model from the nonequilibrium thermodynamic results of Durning and Tabor (1986). Subsequent to that, the key results of previous analyses of the TW model are reviewed; we then describe our numerical methods and finally discuss the numerical results.

The Case II Limit

The unsteady diffusion of fluids in polymers is commonly studied by the 1-D sorption experiment; we focus on sorption, but any unsteady mass-transfer process could be considered. A polymer film occupies the region $0 \le x \le t_i$. The surfaces at $x=0$ and t_i are initially in contact with a large reservoir of a fluid at activity a^-. The system is initially in equilibrium. At time $t=0^+$, the external fluid activity is increased suddenly from a^- to a^+. The fluid then diffuses into the film until a new composition consistent with the equilibrium isotherm is established. Two typical experiments are *interval sorption*, where $a^- > 0$ and $a^+ - a^- \ll 1$ and *integral sorption*, where $a^- = 0$ and a^+ is $\sim$O(1). In either experiment one monitors the sorption kinetics by following the fluid concentration distribution or the weight of fluid absorbed by the film.

A regime of linear behavior can be defined in the limit that the concentration interval (the difference between the initial and final fluid concentrations) is very small, as in an interval sorption experiment with a very small change in activity. Indeed the governing equations from any model could be linearized in this case to supply a linear initial value problem describing the process. Outside of this regime, as in integral sorption experiments, the concentration dependence of the material properties becomes an important feature and the diffusion is nonlinear. In this work, we are primarily concerned with nonlinear viscoelastic diffusion, because its mathematical intractability has clearly impeded engineering-level calculations.

Alfrey et al. (1966) first attempted to organize the viscoelastic behaviors seen in nonlinear 1-D sorptions. They proposed that all nonlinear behaviors lie between two limiting cases: nonlinear Fickian, or "Case I" transport, and "Case II" transport. The limiting behaviors are easily identified in a sorption experiment. If the amount of fluid per unit area, ω, be represented initially by $\omega = kt^n$, where t means time and k and n are constants, then Fickian behavior corresponds to $n = 1/2$, while for Case II transport $n=1$. For intermediate cases, one has $1/2 < n < 1$. Almost all nonlinear sorption experiments conform to this generalization. Consequently, Case II has long been considered a conceptually important limiting case of nonlinear viscoelastic diffusion.

Case II diffusion has the following phenomenological features in 1-D integral sorption experiments:

- A step-like concentration profile develops with a sharp boundary separating a highly swollen region from a nearly dry, typically glassy region.
- The sharp boundary moves into the polymer with a constant velocity causing the amount of fluid absorbed to increase linearly with time.
- A small Fickian "precursor" exists in the dry region ahead of the front.
- There is an initial induction time, during which the sharp boundary is established near the film surface.

A New Derivation of Thomas and Windle's Model for Case II

An important observation was made by Vrentas et al. (1975) on the mechanism of viscoelastic diffusion. For the linear case, they correlated the appearance of non-Fickian behavior with a diffusion Deborah number (*De*), defined as the ratio of the dominant mechanical relaxation time for the polymer/fluid system to its characteristic interdiffusion time. Vrentas et al. observed that transport is Fickian if *De* is either very large or very small. Viscoelastic effects only occur when $De \sim$ O(1). This finding suggests that non-Fickian behavior stems from a coupling between molecular diffusion and the polymer's intrinsic time-dependent response to diffusion induced deformation.

Thomas and Windle (1982) first incorporated the effect of the polymer's retarded mechanical response into a thermodynamic description of diffusion. They assumed that the fluid's diffusion flux is proportional to its chemical potential gradient and postulated that the local fluid potential is affected by the local rate of expansion of the "polymer matrix." Their model can predict all the essential characteristics of Case II transport (Thomas and Windle, 1982; Hui et al., 1987a,b), but it cannot properly describe the linear viscoelastic limit (Durning et al., 1985).

A more recent model, by Durning and Tabor (1986) (DT model), captures the essential features of 1-D linear viscoelastic diffusion. They derived from a well-structured nonequilibrium thermodynamic argument an equation for the fluid flux. The development applies when the polymer suffers only infinitesimal strains during the diffusion. It also assumes a simple functional form for the nonequilibrium free energy consistent with well-accepted molecular-level models of concentrated polymer solutions (transient network model, tube model). The theory correctly predicts 1-D linear viscoelastic behavior observed in interval sorptions without the use of empiricism (Durning, 1985; Mehdizahdeh and Durning, 1990). The framework is attractive for comparison with experiment because of its relatively simple mathematical structure and because all of the physical properties accounting for non-Fickian effects can be measured in independent mechanical experiments. In what follows we consider the application of the DT model to nonlinear transport in one-dimension, where the composition dependence of the transport properties plays a significant role and show that the nonlinear TW model can be recovered as a limiting case for small values of a suitably defined, local Deborah number.

For 1-D sorption, the transport of fluid is governed by the equations of continuity and a constitutive law for the diffusion flux. The equations of continuity have a very simple form in polymer material coordinates if one ignores the volume change on mixing (Billovits and Durning, 1989). In this case the polymer continuity equation is identically satisfied. The fluid continuity equation is:

$$\frac{\partial c}{\partial t} = -\frac{\partial j_{1,\xi}^2}{\partial \xi} \tag{1}$$

where $j_1^2 = \rho_1(v_1 - v_2)$ means the mass flux of the fluid (component 1) relative to the polymer (component 2), v_i means the velocity of component i, ξ is the polymer material coordinate along the diffusion direction, and c is the fluid concentration

per unit volume of polymer [$=\rho_1/(\rho_2\hat{v}_2)$, with ρ_i meaning the mass density of i in the mixture and $\hat{v}_i$ meaning the partial specific volume of i].

A relationship for j_1^2 was derived by Durning and Tabor (1986) using nonequilibrium thermodynamics for a binary mixture with one component (the polymer) having memory. Mixtures concentrated in polymer show very strong changes in the transport properties with fluid content (Vrentas et al., 1975), especially near the glass transition (Vrentas and Duda, 1978; Frick et al., 1990), so it is reasonable to expect a nonlinear regime where polymer strains remain small but the transport properties vary significantly with composition. If one retains all composition dependencies, the theory leads to:

$$j_{1,\xi}^2 = -D(c)\frac{\partial c}{\partial \xi} - D'(c)\frac{\partial}{\partial \xi}\left\{g(c)\left(\int_{-\infty}^{t}\varphi_r(c', t, t')\frac{\partial c}{\partial t'}\,dt'\right)\right\} \quad (2)$$

in one dimension. Here $g(c)$ means $G(c)/G_0$ with $G(c)$ being the instantaneous shear modulus of the mixture, G_0 being $G(c=0)$, $D(c)=D_{12}\ (\rho_2\hat{v}_2)^2$ with D_{12} being the binary mutual diffusion coefficient and

$$D'(c) = D(c)\tilde{v}_1(\partial f/\partial\omega_1)^{-1}\rho\hat{v}_1 G_0/(RT\omega_2) \quad (3)$$

In Eq. 3, RTf is the fluid chemical potential at equilibrium, relative to the pure fluid, $\tilde{v}_i$ means the partial molar volume of component i, and φ_r is the (normalized) shear relaxation modulus of the mixture, measurable by linear viscoelastic mechanical experiments. Note that D, D', g and φ_r are all functions of concentration, c, which introduces important nonlinearities into the governing field equations.

Substituting Eq. 2 into Eq. 1 gives a nonlinear integro-differential equation governing the fluid concentration field, c. To solve this for integral sorption, one needs two boundary conditions and initial conditions. At the polymer/fluid interfaces, the fluid's chemical potential is continuous:

$$\mu_s = \mu_1(\xi=0,\ t) = \mu_1(\xi=t_i,\ t) \quad (4)$$

where μ_s is the fluid's potential in the reservoir and $\mu_1(\xi, t)$ is the potential inside the polymer film. The development leading to Eq. 2 implies that $\mu_1(\xi, t)$ depends on the history of $c(\xi, t)$ through the memory integral in Eq. 2. Thus, Eqs. 4 imply nonlinear integral equations for the surface concentrations. The initial conditions for integral sorption in a dry film are

$$c(\xi,\ t=0) = 0 \text{ for } 0 \le \xi \le t_i \quad (5)$$

In Appendix A we derive a limiting form of Eq. 2 valid for small values of a suitably defined local Deborah number; analogous limiting forms are implied for the boundary conditions. The development presumes only that a simple time-concentration superposition is valid for the mixture. The resulting dimensional expression for the flux is

$$j_{1,\xi}^2 = -D(c)\frac{\partial c}{\partial \xi} - D'(c)\frac{\partial}{\partial \xi}\left(\frac{\eta(c)}{G_o}\frac{\partial c}{\partial t}\right); \qquad De = \frac{\tau(c)D(c=0)}{t_i^2} \ll 1 \quad (6)$$

This is, essentially, the TW model; it turns out to be slow diffusion limit of a more general viscoelastic theory.

In their original formulation, Thomas and Windle put $D(c) \simeq D_o\exp(kc)$, $\eta(c) \simeq \eta_o\exp(-mc)$ and $f \simeq \ln(c/c_e)$, where c_e is the equilibrium value of c in order to capture the essential nonlinearities with simple functional forms. Including these, and introducing the dimensionless quantities:

$$u = \frac{c}{c_e};\quad \zeta = \frac{\xi}{t_i};\quad s = tD_o/t_i^2;\quad K = kc_e;\quad M = mc_e \quad (7)$$

gives the dimensionless initial value problem for integral sorption

$$\frac{\partial u}{\partial s} = \frac{\partial}{\partial \zeta}\left(e^{Ku}\frac{\partial u}{\partial \zeta}\right) + \theta\frac{\partial}{\partial \zeta}\left\{ue^{Ku}\frac{\partial}{\partial \zeta}\left(e^{-Mu}\frac{\partial u}{\partial s}\right)\right\} \quad (8)$$

$$\frac{\partial u}{\partial s} = -\theta^{-1}\ln(u)e^{Mu} \text{ for } \zeta = 0 \text{ and } \zeta = 1 \quad (9)$$

$$u(\xi,\ s=0) = 0 \text{ for } 0 \le \zeta \le 1 \quad (10)$$

where

$$\theta = \frac{D_o\eta_o\tilde{v}_1\rho_{1e}\hat{v}_1}{RTt_i^2} \quad (11)$$

is a dimensionless parameter, related but not identical with De, proportional to the equilibrium volume fraction of liquid, $\rho_{1e}\hat{v}_1$. Equations 9 are the small De limiting forms of the integral equations implied by Eqs. 4. The reader should note that getting the simple dimensionless form of $D'(c)$ shown in Eq. 8, namely ue^{Ku}, requires the approximation $\rho_{1e}\hat{v}_1 \ll \rho_{2e}\hat{v}_2$ in Eq. 3, that is, that the mixture always remain concentrated in polymer; otherwise ue^{Ku} is replaced by $ue^{Ku}/(\rho_{2e}\hat{v}_2 + u\rho_{1e}\hat{v}_1)$. This approximation seems reasonable in view of those taken for $D(c)$, $\eta(c)$ and $f(c)$.

Prior Analyses of the TW Model

Thomas and Windle (1982) formulated the 1-D problem for integral sorption in terms of two coupled field equations, governing the fluid concentration c and the fluid activity a [$=\exp(\mu_1-\mu_1^0)/RT$ where μ_1^0 is the pure liquid potential]. They solved the system numerically by an explicit finite difference method employing a number of assumptions, but did not study the error, stability or convergence characteristics of their numerical scheme. The numerical solutions showed steep concentration fronts moving with nearly constant velocity and linear weight uptake kinetics, features typical of Case II diffusion. They demonstrated numerically that a strong decrease with concentration in the viscosity is essential for the prediction of Case II from the model, and suggested that a diffusion coefficient increasing strongly with concentration is also necessary, although this was not supported by calculations.

Thomas and Windle also studied the surface swelling kinetics by solving Eq. 9 numerically for M in the range $5 \le M \le 20$. For this range in M, they found that the surface concentration increases rather slowly at short times, but then abruptly increases to the equilibrium value after a characteristic "induc-

tion'' time. We refer to this kinetic feature as autocatalytic hereafter.

In a subsequent study of the TW model, Hui et al. (1987a, b) derived analytical asymptotic solutions for the induction time and diffusion front velocity associated with the Case II process. [The 1-D field equations and boundary conditions given by Thomas and Windle (1982) (Eqs. 10–13 in their article) and by Hui et al. (1987b) (Eqs. 8 and 9 in their article) are identical to our Eqs. 8 and 9 except for the definition of the fluid concentration. Both Thomas and Windle and Hui et al. employ the liquid volume fraction; we use $c=\rho_1/\rho_2\hat{v}_2$ which is necessary for a correct mass balance in material coordinates (Billovits and Durning, 1989).] The analysis showed that the surface swelling kinetics governed by Eq. 9 only show autocatalytic behavior if $M>e$, that is, only if the viscosity decreases strongly enough with concentration. In such cases one can define an induction time, s_i, as the intercept of the two apparently linear portions of a $u(\zeta=0, s)\,(\equiv u_s)$ vs. s curve. For $u_s \gg M^{-1}$, Hui et al. found the following approximation:

$$s_i \cong \frac{\theta}{M\ln(M)}, \qquad u_s \gg M^{-1} \tag{12}$$

To analyze the steady-state front motion during the Case II process, Hui et al. took $\eta(c)=\eta_0\exp(-mc)$, but assumed:

$$D(c)=\begin{cases} D_o, & 0\le c<c_c \\ \infty, & c\ge c_c \end{cases} \tag{13}$$

where c_c is a critical concentration. Eq. 13 is not a faithful representation of $D(c)$ (see, for example, Vrentas and Duda, 1978; Frick et al., 1990), however, the assumption leads to neat asymptotic predictions, of a step-exponential concentration profile in the steady state:

$$u=\begin{cases} 1, & 0\le\zeta<\Lambda \\ u_f\exp -v(\zeta-\Lambda), & \Lambda\le\zeta\le 1 \end{cases}$$

where

$$\Lambda=vs; \quad u_f=c_f/c_e; \quad v=Vt_i/D_o=\theta^{-1/2}\beta(M,u_c) \tag{14}$$

Here, Λ is the dimensionless position of the front, c_f is the concentration at the front, V is the velocity of the advancing front (v being the scaled form of V), and $u_c=c_c/c_e$. The value of u_f and the function β depend on the magnitude of V. Two asymptotic cases were developed and are summarized in Appendix B.

The previous works on the TW model show that it captures the essential phenomenological characteristics of the Case II process. Further, the developments in Appendix A suggest that the TW model captures the essential character of a slow diffusion (that is, small *De*) limit of more general first-principles models of viscoelastic diffusion. Consequently, we feel there is considerable value in reexamining the model by more accurate numerical methods than have been used previously.

Numerical Methods for Solution of the TW Model

For a partial differential equation (PDE) with one spatial variable and time, the method of lines (MOL) can be used to convert the PDE into a coupled system of ordinary differential equations (ODEs) in time by first partitioning the spatial domain into subintervals, then discretizing the spatial derivatives using either finite difference methods or finite element methods. The boundary conditions are incorporated into the spatial discretization while the initial conditions are used to start the solution of an associated initial value problem (IVP) for the coupled ODEs. We know that near the limit of Case II diffusion, steep concentration gradients and a traveling wave are expected. This demands that the ODE integrator be able to handle ''stiff'' problems effectively (the notion of stiffness is explained briefly in a subsequent section). Finlayson (1980) has shown that for stiff, nonlinear PDEs in a finite spatial domain, finite element discretization methods generally outperform the finite difference methods in both accuracy and computation efficiency. Therefore, for Eq. 8, we chose a finite element method for the spatial discretization and adopted an ODE integrator (LSODI) designed to handle stiff IVP problems effectively.

Orthogonal collocation on hermite cubics

Collocation methods are a class of finite element schemes which seek approximate solutions in the form of a sum of piecewise continuous polynomial functions. For the reasons given by Fu (1992), we chose the Hermite cubic interpolation functions. So, in our case, the dimensionless concentration u is approximated by the trial solution, $\tilde{u}$

$$u(\zeta,s)\cong\tilde{u}(\zeta,s)=\sum_i\left[\alpha_i^{(1)}(s)\nu_i(\zeta)+\alpha_i^{(2)}(s)\sigma_i(\zeta)\right] \tag{15}$$

where the range of i will be defined below. The ''value'' function ν_i and the ''slope'' function σ_i are specified cubic polynomials in ζ (Davis, 1984; Fu, 1992). Their properties are such that $\alpha_i^{(1)}(s)$ gives the value of $\tilde{u}$ at ζ and s and $\alpha_i^{(2)}(s)$ gives the slope of $\tilde{u}$ at ζ and s. A set of coupled, ordinary differential equations for the unknown α (a vector of all α's) can be generated from an error minimization principle (Burnett, 1987). Define a residual function $r(u,\xi,s)$ for Eq. 8:

$$r(u,\zeta,s)=\frac{\partial u}{\partial s}-\frac{\partial}{\partial\zeta}e^{Ku}\frac{\partial u}{\partial\zeta}-\theta\frac{\partial}{\partial\zeta}ue^{Ku}\frac{\partial}{\partial\zeta}e^{-Mu}\frac{\partial u}{\partial s}$$

and denote the residual associated with $\tilde{u}$ by $R(\zeta, s; \alpha)\equiv r(\tilde{u}, \zeta, s)$. The error due to the approximation $\tilde{u}$ is minimized by calculating the $\alpha_i^{(1)}(s)$ and $\alpha_i^{(2)}(s)$ that force

$$\int_0^1 R(\zeta, s; \alpha)\omega_k(\zeta)d\zeta=0 \tag{16}$$

where the ω_k are a set of weighting functions. If this set is sufficiently large, Eqs. 16, with appropriate initial conditions, define an IVP for the unknown α. In the orthogonal collocation method, $\omega_k(\zeta)=\delta(\zeta-\zeta_k^c)$, with δ being the Dirac delta function and ζ_k^c being a set of collocation points.

In the application of orthogonal collocation one partitions the ζ domain ($0\le\zeta\le 1$) into nx elements (subintervals). Let ζ_i, such that $0=\zeta_1<\zeta_2<\ldots\zeta_j<\zeta_{nx+1}=1$, define the interelement boundaries. Then, the summation in Eq. 15 ranges from 1 to

$nx+1$, and the total number of time-dependent unknown α(s) is $2nx+2$. Therefore, orthogonal collocation on Hermite cubics requires that Eq. 16, with $\omega_k(\zeta)=\delta(\zeta-\zeta_k^c)$, be applied at $2nx+2$ specific spatial points: Two collocation points in each element (see subsequent discussion) plus two boundary points ($\zeta=0$, 1). Substituting Eq. 15 into Eq. 16 and evaluating the result at the interior collocation and boundary points gives $2nx+2$ ODEs for the unknown α(s). Equations 10 and 15 supply initial conditions for the ODE's to define an IVP.

An effective IVP solver

The most important considerations in selecting a numerical method for an IVP governed by a system of ODEs are stability, convergence and accuracy. Linear multistep methods are among the best with respect to these features (Davis, 1984). Consider the system of N first-order ODEs:

$$\dot{y}=f(y,t);\quad 0\le t\le\infty;\quad y(0)=y_o$$

where $y=[y_1, y_2, \ldots, y_N]^T$ is the N dimensional, column vector of dependent variables. Denote the numerical approximations to y and $\dot{y}$ at the current time, t_{n-1}, by y_{n-1} and $\dot{y}_{n-1}$, respectively. The increments t_n-t_{n-1} are the time step sizes, h_n. Linear multistep methods use the linear combinations of the solution and derivative values at more than one past point, that is, y_i and $\dot{y}_i$ for $i\le n-1$, to determine an approximation at the next time, y_n. They are represented by the formula:

$$y_n=\sum_{j=1}^{k_1}\alpha_j y_{n-j}+h\sum_{j=0}^{k_2}\beta_j\dot{y}_{n-j} \tag{17}$$

where $\dot{y}_{n-j}$ denotes $f(y_{n-j}, t_{n-j})$. The quantities k_1, k_2, α_j and β_j are constant coefficients whose values define a particular method. The above formula defines an order q method, where q usually corresponds to $\max(k_1, k_2)$. The method is explicit if $\beta_o=0$, but implicit otherwise. In the implicit case, Eq. 17 is solved by first approximating y_n in a predictor step based on an explicit method, and then in a corrector step employing an iterative scheme to find a better solution of Eq. 17.

Consider the conditions needed to ensure that a linear multistep scheme will be stable in the sense of damping initial numerical errors. A detailed stability analysis for linear problems has been done (see, for example, Gear, 1971; Hindmarsh, 1972) and one can apply the results to a locally linearized form of a nonlinear problem to understand its stability requirements qualitatively. Hindmarsh's results for the linear ODE, $\dot{y}=\lambda y$ where λ is complex, indicate that, for any linear multistep integration scheme, there exists a region of absolute stability S in the complex plane of $h\lambda$. The conditions for absolute stability of N linear, uncoupled ODE's with eigenvalues λ_j ($j=1, 2, \ldots, N$) derived by local linearization and linear transformation of a nonlinear problem are that all $h\lambda_j$ lie within S for the multistep method under consideration. Obviously, it is advantageous to select a method with the largest possible S to avoid instability. For backward difference formulation (BDF) methods of order q, S is all of the left half-plane for $q=1$ or 2, and all of the left half plane except for two narrow strips along the imaginary axis for $3\le q$ (Hindmarsh, 1991; Gear, 1971), so these methods are attractive from the point of view of stability.

An important characteristic influencing the efficiency of a numerical solution is the "stiffness" of the problem. The stiffness of the ODE system $\dot{y}=f(y, t)$ refers to the spread of characteristic time constants defined as $\tau_i=-1/Re(\lambda_i)$ where the λ_i are the eigenvalues of the Jacobian matrix of $f(y, t)$. For large values of the ratio $\max|Re\lambda_i|/\min|Re\lambda_j|$ the system is considered stiff. For such problems the use of a numerical method with finite S may severely impede computational efficiency since the step size h_n will be restricted to $h_n\sim O(1/|\max\lambda_i|)$, which may be intolerably small in practice. Clearly, methods with largest possible S are required for stiff problems; BDF methods are therefore among the best for efficient solution of stiff IVPs.

The ODE system associated with the TW model is stiff for conditions giving Case II transport. This is because the eigenvalues of the ODE system depend on the diffusivity $D(c)$ and viscosity $\eta(c)$ appearing in the PDE and these can vary over several orders of magnitude with concentration in the Case II limit. From the above, an integrator employing a BDF scheme should be a useful method. LSODI, developed by Painter and Hindmarsh (1982), is a powerful IVP solver which can implement the BDF method of order q ($k_1=q$, $k_2=0$, $\beta_o>0$) for systems in the implicit form:

$$A(y,t)\cdot\dot{y}=G(y,t) \tag{18}$$

LSODI solves Eqs. 18 using Newton's method in the corrector step. Details of the computational techniques employed by LSODI are discussed by Painter and Hindmarsh (1982) and by Fu (1992).

A code for the TW model

The foregoing discussion indicates that the MOL using collocation on Hermite cubics for the spatial discretization and the BDF method for the time integration should provide a good combination of stability and computational efficiency in solving the TW Model. We developed a FORTRAN code to implement this calculation. The code defines an ODE system for the TW model resulting from the spatial discretization. It includes LSODI user-supplied subroutines and calls LSODI as a subroutine for the BDF time integration. The structure of the code is shown in Figure 1. This structure would apply for the solution of any model of 1-D sorption; only the definitions of A and G are model specific.

Before describing how we formulated A, G and the initial values of y for the TW model, consider the choice of the collocation points. It can be shown (Davis, 1984; Burnett, 1987) that the choice giving the highest accuracy for Hermite cubics [$O(h_j^4)$] in the case of PDE's second order in the spatial derivatives is:

$$\zeta_{j1}^c=\zeta_j+(h_j/2)[1-(1/\sqrt{3})]$$

for the first collocation point in the jth subinterval, and

$$\zeta_{j2}^c=\zeta_j+(h_j/2)[1+(1/\sqrt{3})]$$

for the second collocation point in the jth subinterval. Here $h_j=\zeta_{j+1}-\zeta_j$ means the size of jth subinterval. We chose these collocation points in our application.

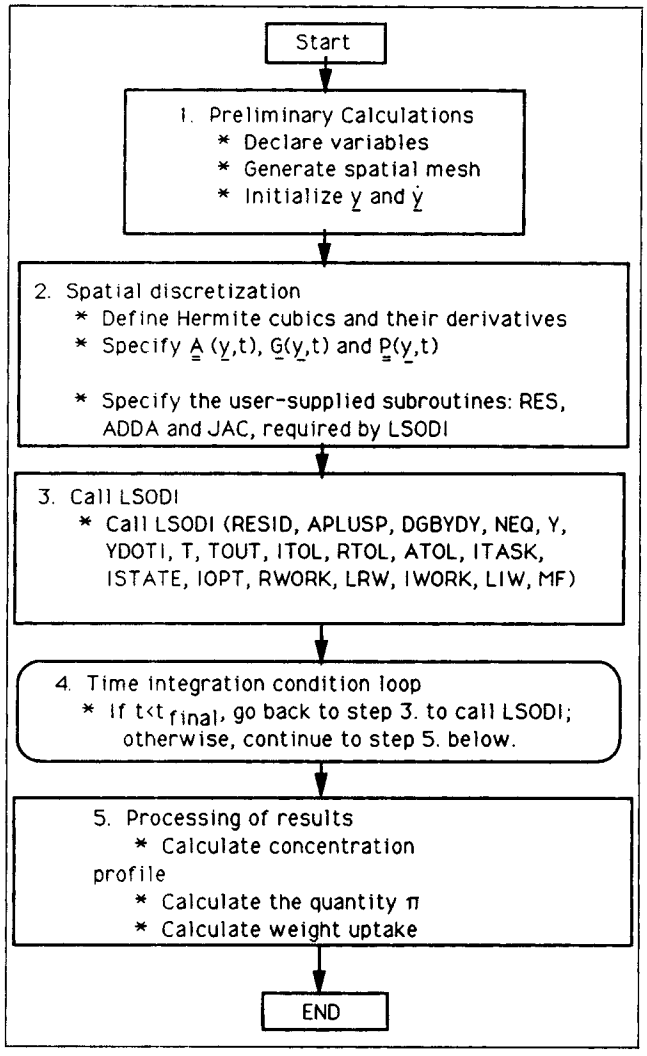

Figure 1. Structure of the FORTRAN Code.

Now consider the formulation of A and G in Eq. 18 for the TW model. Equation 8 was rearranged so that all time derivatives appear on the lefthand side:

$$\frac{\partial u}{\partial s}-\theta e^{u(K-M)}\left\{u\frac{\partial u^3}{\partial\zeta^2\partial s}-Mu\frac{\partial u}{\partial s}\frac{\partial^2 u}{\partial\zeta^2}+[u(K-2M)+1]\frac{\partial u}{\partial\zeta}\frac{\partial^2 u}{\partial\zeta\partial s}\right.$$
$$\left.+M[u(M-K)-1]\left(\frac{\partial u}{\partial\zeta}\right)^2\frac{\partial u}{\partial s}\right\}=e^{Ku}\left\{\frac{\partial^2 u}{\partial\zeta^2}+K\left(\frac{\partial u}{\partial\zeta}\right)^2\right\} \quad (19)$$

Then, the trial solution, $\tilde{u}$, was substituted for u and all of the differentiations were carried out. Letting y represent a vector of the α's,

$$y(s)=\{y_1, y_2, \ldots, y_{2nx+1}, y_{2nx+2}\}^T$$
$$=\{\alpha_1^{(1)}, \alpha_1^{(2)}, \alpha_2^{(1)}, \alpha_2^{(2)}, \ldots, \alpha_{nx+1}^{(1)}, \alpha_{nx+1}^{(2)}\}^T$$

then A is the $(2nx+2)$ by $(2nx+2)$ matrix of the coefficients of the terms linear in $\dot{y}$ on the left in Eq. 19 and in the boundary conditions, Eqs. 9, after introducing $\tilde{u}$. G is the column vector of size $(2nx+2)$ corresponding to the righthand side of Eq. 19 after introducing $\tilde{u}$. A has a banded structure and its elements

Table 1. Properties Used in the Estimation of θ for the Typical Case*

Diffusivity of methanol in PMMA at 24°C	$D_o=10^{-14}$ [M²/s]
Viscosity of PMMA at 24°C	$\eta_o=2\times10^{14}$ [Ns/M²]
Molar volume of methanol	$\tilde{v}_1=4.05\times10^{-5}$ [M³/mol]
Initial PMMA film thickness	$l_i=10^{-3}$ [M]
Equilib. vol. frac. of MeOH in PMMA at 24°C	$\hat{v}_1\rho_{1e}=0.23$
Gas constant	$R=8.314$ [J/mol·K]
Temperature	$T=297$ [K]
Calculated value	$\theta=7.5447\times10^{-3}$

*Taken from Thomas and Windle (1982).

are strong functions of y; G is also strongly nonlinear in y. Explicit formulae for A and G for the TW model are given by Fu (1992) together with the FORTRAN code implementing the integration.

Numerical Results and Discussion

We first discuss a "typical" case, where the model parameters correspond approximately to the system liquid methanol in poly(methylmethacrylate) PMMA, where Case II transport is known to occur (Thomas and Windle, 1982). Table 1 lists values of all the physical properties needed to estimate θ. They correspond to liquid methanol in contact with 1-mm-thick PMMA plates at room temperature. The value of θ was rounded from 0.0075 to 0.01 for the following typical calculation. The values of K and M were set to 5 to mimic the characteristically strong concentration dependence of the diffusivity and viscosity in polymer/fluid systems. Actual values of K and M for this system at room temperature are larger according to Thomas and Windle (1982).

For the typical case, the number of subintervals, nx, was set to 30 giving a total of 62 collocation points. The results for the surface concentration, governed by Eq. 9, are plotted in Figure 2a; the concentration distributions are shown in Figure 2b.

In Figure 2a, the surface concentration u_s shows a weakly autocatalytic response (note mild upward curvature). From the intercept of the two apparently linear portions one can identify an induction time, $s_i=8.8\times10^{-4}$. Beyond s_i, u_s increases rapidly and then later relaxes slowly to equilibrium. The surface response calculated in Figure 2a is consistent with the results of Thomas and Windle (1982) and of Hui et al. (1987a) for similar conditions. The physical interpretation is as follows. Following the initial step increase in fluid activity at the surface, fluid accumulates very slowly because of the retarded dilational response of the dry polymer "matrix" at the surface to the imposed thermodynamic force. As fluid accumulates, the viscosity governing the rate of dilation falls precipitously, accelerating the rate of accumulation. Eventually, the driving force decays to zero, the rate of fluid accumulation decays and u_s relaxes slowly to equilibrium.

Figure 2b shows the dimensionless concentration, u, vs. the dimensionless distance, ζ, as dimensionless time, s, increases until equilibrium. Three important features appear in Figure 2b. The surface swelling process just discussed is evident: u_s increases with s from 0 to 1. After u_s reaches 1, a step-like profile develops and moves into the film. This occurs for dimensionless times in the range $0.002<s<0.004$ and is the Case

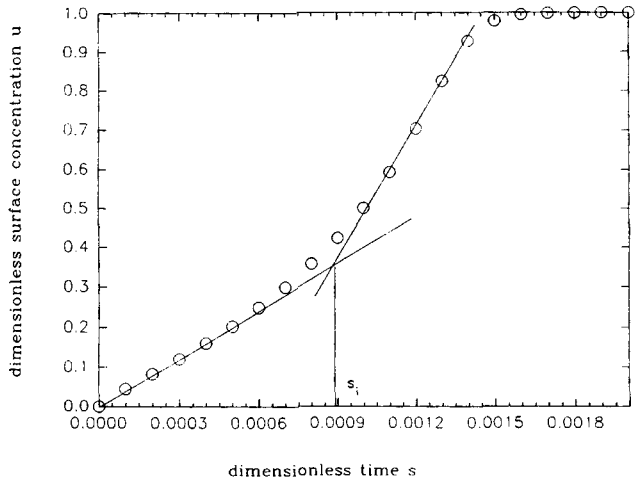

Figure 2a. Surface swelling kinetics (Eq. 9) with $\theta = 0.01$ and $M = 5$.

The induction time s_i is 0.00088.

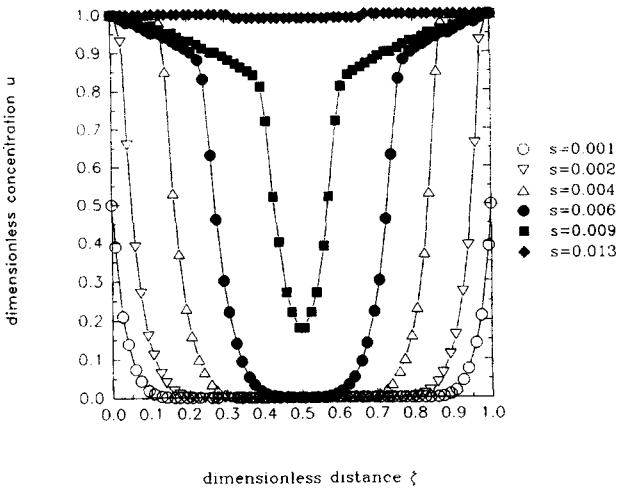

Figure 2b. Concentration profiles for the TW model (Eqs. 8-10) with $\theta = 0.01$, $M = K = 5$, $nx = 30$.

Legend indicates times s.

II process. The final interesting feature is the development of a concentration gradient behind the steep front at long times. This indicates that the Case II process eventually becomes diffusion controlled, as has been observed experimentally in thick samples (Hopfenberg, 1978) and as is predicted in the phenomenological modeling of viscoelastic diffusion by Astarita and Sarti (1978). So, the typical case shows all the well-known features of 1-D, nonlinear, viscoelastic diffusion very near the Case II limit.

A series of solutions with finer grid spacings (that is, progressively larger nx) was used to check whether a sequence of improved approximations produced by our code converged to a common limit, that is, whether our numerical solution is convergent. Profiles were computed using the same parameters as in Figure 2b, but with $nx = 50$ and 100; these were superimposable on Figure 2b, indicating that the code produced convergent solutions of the model. For the rest of the calculations discussed, $nx = 30$ is used. The effect of the time step-size was not studied systematically since the user supplied value is adjusted internally by LSODI to achieve a compromise between accuracy and efficiency.

The quantity $\Pi = e^{-Mu}(\partial u/\partial s)$ represents the dimensionless, nonequilibrium contribution to the local fluid chemical potential implied by Eq. 6. The distribution of Π accompanying Figure 2b is shown in Figure 2c. Initially Π shows an extremely sharp peak ($\Pi \simeq 130$) near the surface. During the Case II process the step-like concentration profiles are proceeded by sharp pulses in Π. As a concentration gradient develops behind the front, these broaden and relax and eventually vanish as equilibrium is reached.

The dimensionless weight uptake, $W(s) = \int_0^1 u(s,\zeta)d\zeta$, was calculated using Simpson's rule (Carnahan et al., 1975). $W(s)$

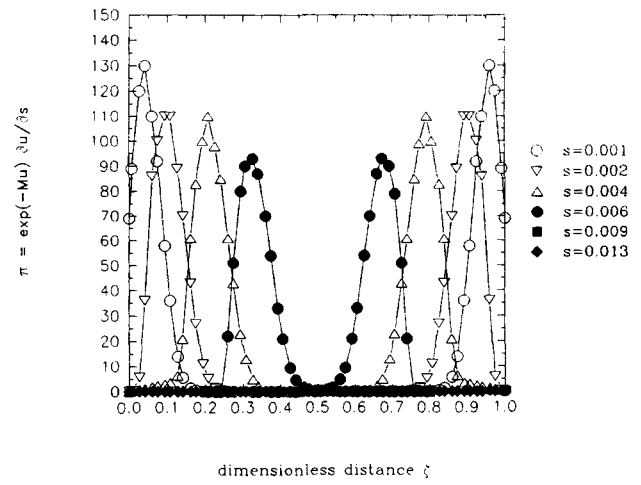

Figure 2c. Quantity Π for the TW model (Eqs. 8-10) with $\theta = 0.01$, $M = K = 5$, $nx = 30$.

Legend indicates times s.

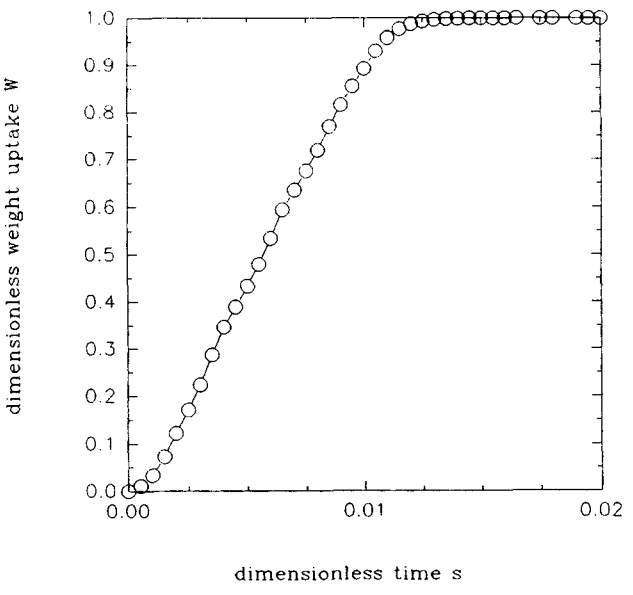

Figure 2d. Weight uptake kinetics for the TW model (Eqs. 8-10) with $\theta = 0.01$, $M = K = 5$, and $nx = 30$.

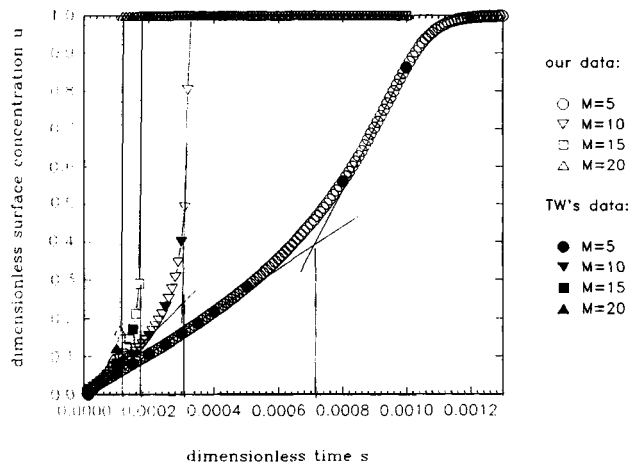

Figure 3a. Dependence of surface swelling kinetics (Eq. 9) on M with θ fixed at 0.0075.

Thomas and Windle's data (1982) are also plotted for comparison. Legend indicates values of M.

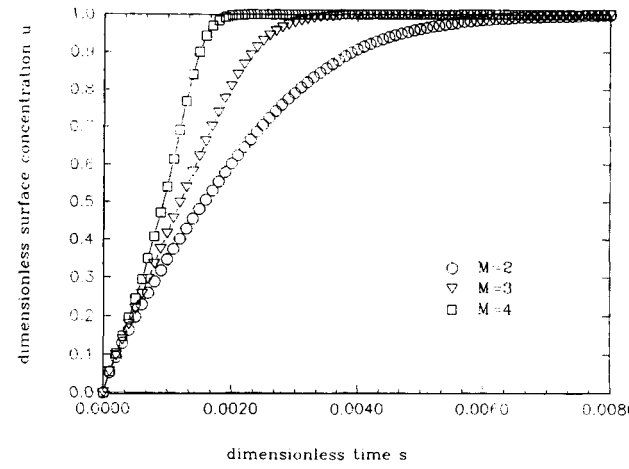

Figure 3b. Dependence of surface swelling kinetics (Eq. 9) on M with θ fixed at 0.0075.

for the typical case is given in Figure 2d; it is clearly linear in time after the induction period for W up to 0.6–0.7.

In all, the results for concentration profiles, the quantity Π and the weight uptake for the typical case are qualitatively consistent with Thomas and Windle's calculations and clearly characteristic of nonlinear viscoelastic diffusion near the Case II limit. In what follows we make quantitative comparisons with previous work on the TW model and systematically explore the effects of the parameters θ, M and K for values in the neighborhood of the typical case. Before proceeding however, a few pragmatic remarks are relevant.

All the calculations were done on a 33 MHz 386 PC computer with a math coprocessor. The compilation and execution of the code were done with a commercial FORTRAN compiler combined with a DOS extender. The execution time for a run ranged from approximately 10 min for weak nonlinearity to about 10 h for strong nonlinearity. By trial and error we discovered that there is a limited range of θ, M and K for which the code gives solutions. These were found to be: $0 \le \theta \le 10$, $0 \le M \le 5$ and $0 \le K \le 5$. Outside of this range, the calculation would become unstable during a run and eventually diverge. Also, there exist some combinations of θ, M, K and nx within the above range which proved to be problematic. They are: $\theta = 0.01$, $M = 5$, $K = 0$ for any nx; $\theta = 0.01$, $M = 0$, $K = 5$, for any nx; $\theta = 0.01$, $M = K = 5$ for $nx < 30$; $\theta = 0.0075$, $M = K = 5$ for any nx. These failures could be due to a violation of unspecified requirements by LSODI in the user supplied subroutines for M and/or $K \ge 5$, or a violation of stability criteria for the solution of the ODE system when M or $K \ge 5$. Notwithstanding this, we can have some meaningful discussions of the effects of θ, M, and K within the stable ranges. Strategies for overcoming the current limitations of the code are discussed later.

A finite rate of increase in surface concentration, u_s, is a well-known feature of non-Fickian sorption. As discussed previously, Thomas and Windle (1982) examined $M \ge 5$ numerically and found an autocatalytic response for u_s; in such cases, one can define an induction time s_i (for example, Figure 2a). Recall also that Hui et al. (1987a) developed an asymptotic result for s_i for sufficiently large M (Eq. 12). We performed a series of calculations to compare with Thomas and Windle's and to test Hui et al.'s result for the effect of M. (There is no need to probe the effect of θ on s_i numerically since Eq. 9 indicates that the effect of changing θ is just to rescale time, which immediately gives that s_i is proportional to θ, in agreement with Eq. 12.) We calculated u_s vs. s for $M = 5$, 10, 15 and 20 with θ fixed to 0.0075. Our results along with those of Thomas and Windle (1982) appear in Figure 3a; the two calculations agree perfectly. All the plots show autocatalytic response and permit calculation of induction times. Calculations for $M = 2$, 3 and 4 with $\theta = 0.0075$ were also done (see Figure 3b). For $M = 2$ or 3, an induction time cannot be determined since u_s shows no upward curvature; $M = 4$ shows only weak autocatalytic response. The appearance of the induction time for $M > 3$ confirms the analysis of Hui et al. (1987a). The induction times for $M \ge 5$ were measured by linear regression as illustrated in Figure 2a and are collected in Table 2. A log-log plot of s_i vs. $[Mln(M)]$ showed good linearity and gave the regression slope of -0.886 ± 0.038, indicating that $s_i \sim [Mln(M)]^{-1}$ to within numerical error, in agreement with Eq. 12. So, our numerical study of the influence of M on s_i agrees exactly with Thomas and Windle's (1982) numerical work and confirms Hui et al.'s (1987a) analytical asymptote.

Unfortunately, we could not compare our results for $u(\zeta, s)$ directly to Thomas and Windle's due to the limited range of M and K accessible with our code. However, we could qualitatively compare our results for the case $\theta = 0.0075$, $M = 5$, $K = 4$ to Thomas and Windle's calculation for $\theta = 0.0075$, $M = 5$ and $K = 6.215$. They both show sharp fronts, although our calculations show that a significant gradient develops behind the moving front at long times, which does not appear in Thomas and Windle's result. Thomas and Windle's data show

Table 2. Induction Times s_i as a Function of M with θ Fixed at 0.0075

No.	M	$s_i \times 10^4$
1	5	7.15
2	10	3.05
3	15	1.75
4	20	1.20

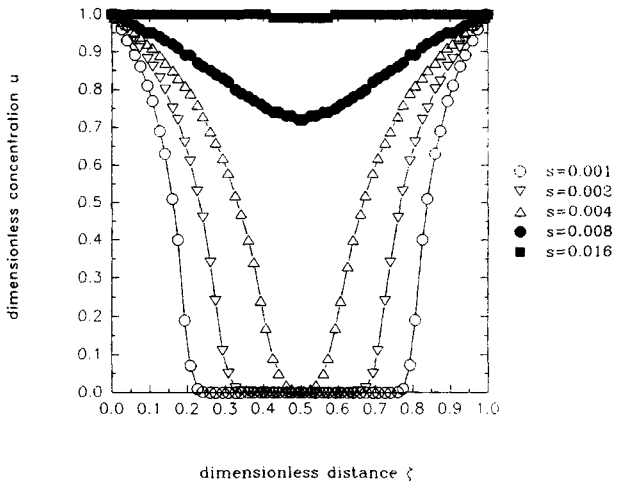

Figure 4a. Concentration profiles for the TW model (Eqs. 8-10) with $\theta = 0.0001$, $M = K = 4$, and $nx = 30$.

Legend indicates times s.

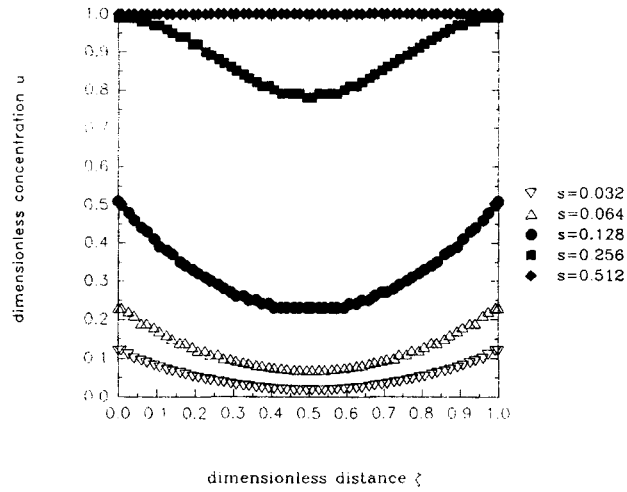

Figure 4b. Concentration profiles for the TW model (Eqs. 8-10) with $\theta = 1$, $M = K = 4$, and $nx = 30$.

Legend indicates times s.

slightly steeper profiles and reach equilibrium somewhat faster. These differences are likely due to the disparity in K between the two calculations (their value is 1.56× ours) and the difference in numerical schemes.

The effect of θ on the concentration profiles was studied by varying its value over 4 orders around the typical value with M and K fixed at 4. The concentration profiles shown in Figures 4a and 4b correspond to the two extreme values of θ, 10^{-4} and 1, respectively; the associated weight uptake curves appear in Figures 5a and 5b. From Eq. 11, θ represents the ratio of timescales for flow of the dry polymer under a stress $\sim O(RT/\bar{v}_1)$ to the timescale for molecular diffusion of the fluid through the dry, glassy polymer a distance equal to the film half thickness, t_i; note that $\theta \sim t_i^{-2}$. The simplest physical interpretation of varying θ with the properties M and K fixed is of varying the film thickness. In particular, one can interpret that increasing θ by four orders corresponds to decreasing the film thickness by two orders. We therefore anticipate that as θ increases beyond the typical value of 10^{-2}, the evolution of concentration profiles within the film becomes dominated by the surface concentration kinetics, as one would expect in experiments on methanol sorption in extremely thin (<0.1 mm) PMMA films. Conversely, as θ decreases below 10^{-2}, we anticipate a trend toward diffusion control of the concentration profiles. Figures 4 and 5 verify this intuition. For $\theta = 10^{-4}$, corresponding to thick films, diffusion control is evident; concentration profiles (Figure 4a) show large gradients near the surface and possess downward curvature. With the largest $\theta(=1)$, corresponding to very thin films, the kinetics of surface swelling clearly control the concentration profiles (Figure 4b) and the weight uptake closely resembles the surface kinetics (Figure 5b).

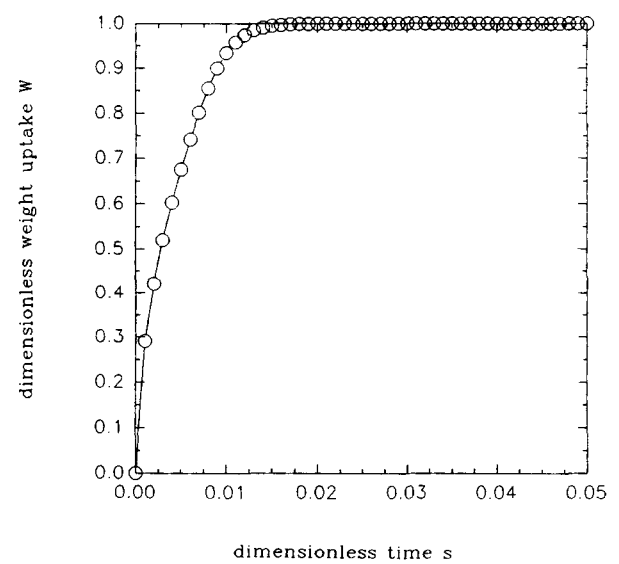

Figure 5a. Weight uptake kinetics for the TW model (Eqs. 8-10) with $\theta = 0.0001$, $M = K = 4$, and $nx = 30$.

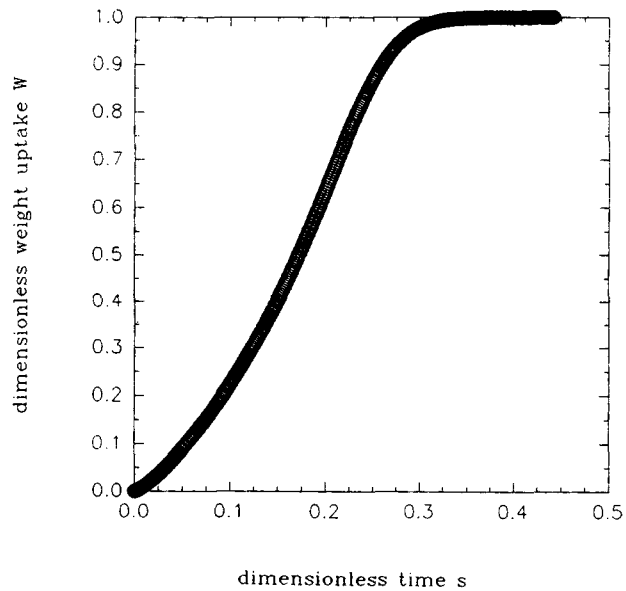

Figure 5b. Weight uptake kinetics for the TW model (Eqs. 8-10) with $\theta = 1$, $M = K = 4$, and $nx = 30$.

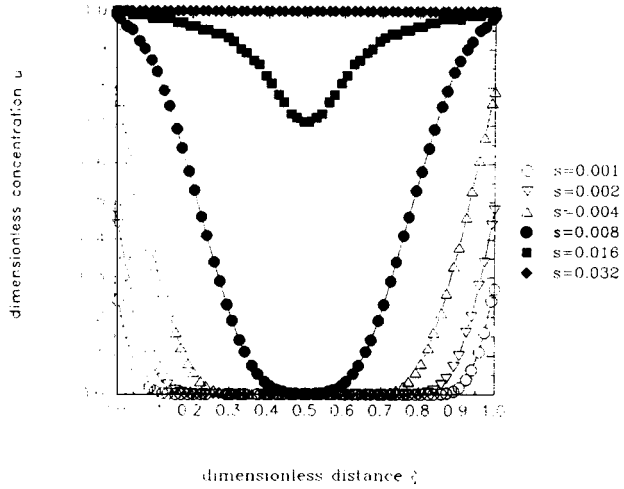

Figure 6a. Concentration profiles for the TW model (Eqs. 8-10) with $\theta = 0.01$, $M = 2$, $K = 5$, and $nx = 30$.

Legend indicates times s.

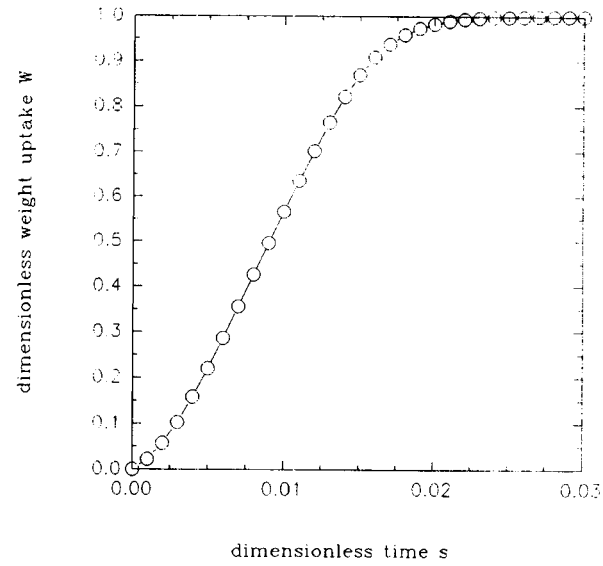

Figure 6b. Weight uptake kinetics for the TW model (Eqs. 8-10) with $\theta = 0.01$, $M = 2$, $K = 5$, and $nx = 30$.

Next, the effects of the nonlinearity in the viscosity were studied by varying M between with θ and K fixed at 0.01 and 5, respectively; Figures 6, 7, 2b and 2d show representative results. In agreement with Thomas and Windle's (1982) study, we find that the nonlinearity in the viscosity function is critical to the appearance of Case II behavior. When this nonlinearity is weak (for example, $M = 2$ as in Figure 6), the features characteristic of Case II are absent. Figure 6a shows the concentration profiles for this case; there is no evidence of a traveling front. Figure 6b shows the corresponding weight uptake vs. time. The plot shows weak upward curvature for $W(s)$ up to 0.4-0.5 reminiscent of the surface kinetics rather than the linearity characteristic of Case II. Indeed, Figures 6 and 7 show that the features characteristic of Case II, which are very clear in Figure 2b, disappear when M falls below 3 to 4. This corresponds to the suppression of an autocatalytic response in the surface concentration kinetics. Evidently, autocatalysis is a crucial nonlinear feature for the prediction of Case II.

We also considered the influence of the nonlinearity in the diffusion coefficient on the predictions. Thomas and Windle's original numerical study (1982) showed that with constant diffusivity and with $\theta = 0.0075$ and $M = 15$, concentration profiles still showed the discontinuous front characteristic of Case II transport although a large gradient readily developed behind the front in this case. This slows the front with time thereby precluding weight uptake linear with time as is characteristic of Case II. They suggested that while the nonlinearity in the viscosity function is crucial for the appearance of a sharp front, prediction of the Case II process also requires a strongly nonlinear diffusion coefficient, increasing with concentration. We attempted to explore this question further. Figures 8 and 9, together with Figures 2b and 2d, show the influence of K on

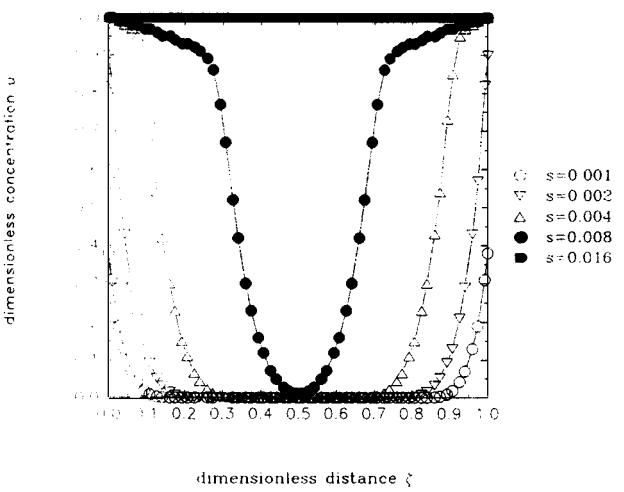

Figure 7a. Concentration profiles for the TW model (Eqs. 8-10) with $\theta = 0.01$, $M = 4$, $K = 5$, and $nx = 30$.

Legend indicates times s.

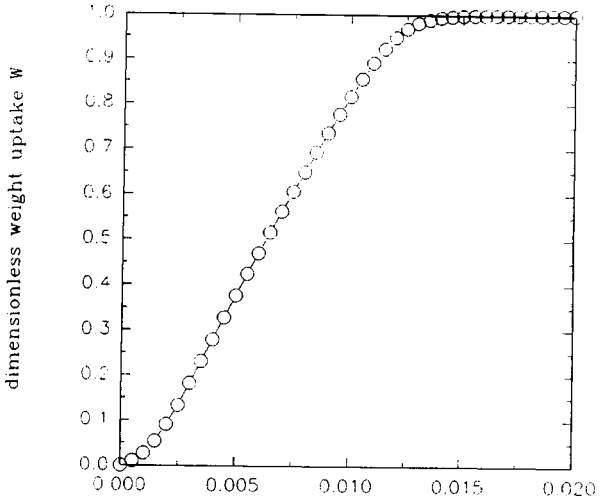

Figure 7b. Weight uptake kinetics of the TW model (Eqs. 8-10) with $\theta = 0.01$, $M = 4$, $K = 5$, and $nx = 30$.

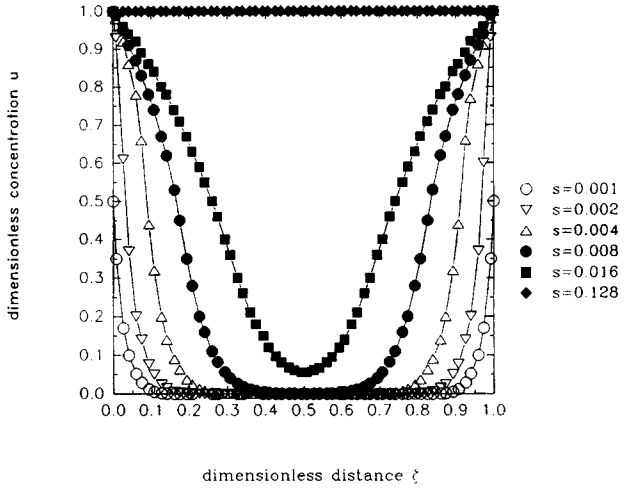

Figure 8a. Concentration profiles for the TW model (Eqs. 8-10) with $\theta = 0.01$, $M = 5$, $K = 2$, and $nx = 30$.
Legends indicate various times s.

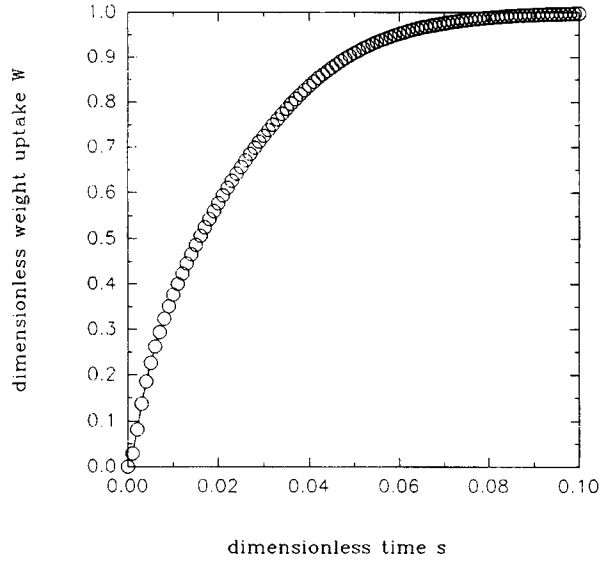

Figure 8b. Weight uptake kinetics for the TW model (Eqs. 8-10) with $\theta = 0.01$, $M = 5$, $K = 2$, and $nx = 30$.

the behavior with θ and M fixed at 0.01 and 5, respectively. As K decreases from 5 to 2, the front disappears. At the same time, the weight uptake curves change from linear with s (Figure 2d) to more nearly linear with $\sqrt{s}$ (Figure 8b), a Fickian feature. These results clearly indicate that K must be sufficiently large for the prediction of Case II and support Thomas and Windle's suggestion that a diffusion coefficient strongly increasing with concentration an essential feature for Case II.

The foregoing calculations show very clearly that in order to predict Case II from a model based on Eq. 6, one must have both a diffusion coefficient increasing strongly with fluid concentration and a viscosity decreasing strongly with concentration.

Hui et al. (1987b) developed simple, asymptotic formulas for the steady front velocity during Case II (Eqs. 14, B1 and B2). These, however, were derived using the assumption of a sudden divergence of the diffusion coefficient with fluid concentration (Eq. 13). We observed Case II profiles under the conditions $\theta = 0.01$, $M = K = 5$ (Figure 2b) without adopting Eq. 13, and were interested to see whether the simple functional forms given by Hui et al. remained valid. Verification of this would enable simple analysis of experimental results on systems displaying Case II features over a broad range of conditions without having to test the validity of Hui et al.'s assumptions for the system of interest.

Since our calculations explore the range $M \leq 5$, only the "slow front" limit (Eq. B2) could be checked directly for the effect of M on the dimensionless front velocity (in fact, for $M \leq 5$, Eq. B1 gives unphysical predictions). According to Eq. 14, the dimensionless front velocity v is proportional to $\theta^{-1/2}$ when $\beta(M, u_c)$ (that is, M) is fixed. Also, from Eqs. 14 and

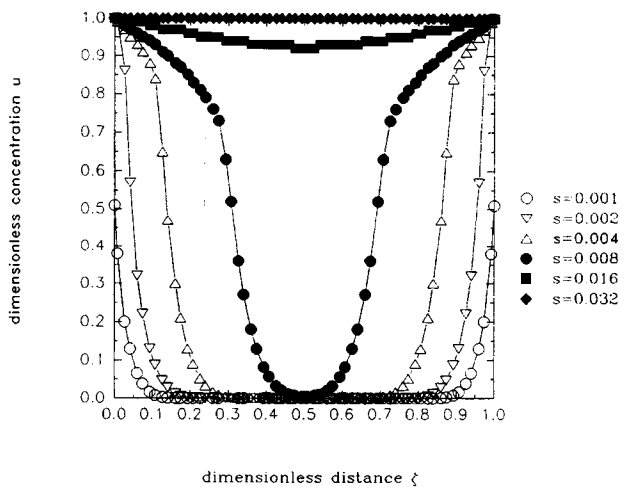

Figure 9a. Concentration profiles for the TW model (Eqs. 8-10) with $\theta = 0.01$, $M = 5$, $K = 4$, and $nx = 30$.
Legend indicates times s.

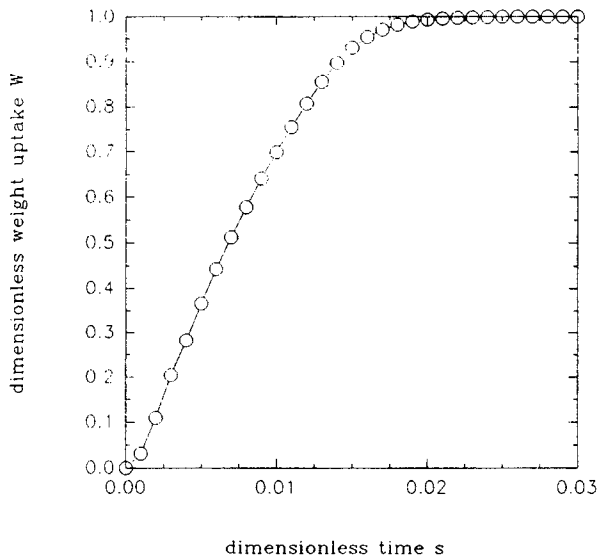

Figure 9b. Weight uptake kinetics for the TW model (Eqs. 8-10) with $\theta = 0.01$, $M = 5$, $K = 4$, and $nx = 30$.

Table 3. Dependence of the Dimensionless Diffusion Front Velocity v on the Dimensionless Number θ with M and K Fixed at 5

#	θ	v_c	v_w
1	0.01	56±5	48.0±2.0
2	0.0125	52±5	43.0±2.0
3	0.015	47±5	40.0±2.0
4	0.0175	42±5	37.0±2.0
5	0.02	40±5	34.0±2.0
6	0.0225	38±5	32.0●2.0
7	0.025	35±5	30.0±2.0

v_c = front velocity measured by tracking the steady motion of the concentration fronts

v_w = front velocity measured from linear regression slopes of the linear portion of weight uptake curves

Table 4. Dependence of Dimensionless Diffusion Front Velocity v on M with θ and K Fixed at 0.01 and 5*

#	M	v_c	$M/(v_c^2\theta)$	v_w	$M/(v_w^2\theta)$
1	3	47±5	0.1358	38.0±2.0	0.2121
2	3.25	50±5	0.1300	40.0±2.0	0.2098
3	3.5	52±5	0.1294	41.0±2.0	0.2095
4	3.75	53±5	0.1335	42.0±2.0	0.2094
5	4	54±5	0.1372	44.0±2.0	0.2084
6	4.25	55±5	0.1405	45.0±2.0	0.2087
7	4.5	56±5	0.1435	46.0±2.0	0.2098
8	4.75	56±5	0.1515	47.0±2.0	0.2112
9	5	56±5	0.1594	48.0±2.0	0.2140

*For v_c and v_w, see remarks at the bottom of Table 3.

B2 for the slow front limit, v is proportional to $[\exp(Mu_c)]^{1/2}$ when θ is fixed.

For Case II, the dimensionless rate of fluid uptake during steady-state front propagation is $dW/ds = 2v$. So, the velocity v can be determined from the regression slope of the linear portion of the weight uptake curve. This value can be checked by direct tracking of the steady motion of the corresponding concentration profiles.

Table 3 gives values as a function of θ of the dimensionless front velocity, $v_w = (1/2)dW/ds$, determined from the regression of the weight uptake kinetics, and of v_c, determined by tracking the steady motion of the concentration fronts. The values of v_w and v_c are reasonably close, although v_w has somewhat better accuracy. For the following we use v_w and drop the subscript for convenience. A log-log plot of v vs. θ^{-1} appears in Figure 10; a linear regression slope of 0.511 ± 0.006 was found indicating $v \sim \theta^{-0.511 \pm 0.006}$ which is very near the asymptotic prediction by Hui et al. (1987b).

The effect of M on the front was studied in the range $3 \le M \le 5$ with θ and K fixed at 0.01 and 5, respectively. This ensures the condition $\exp(-Mu_c) \sim O(1)$ for $u_c \sim O(1)$ as required by the asymptotic analysis. Table 4 gives M, v_c and v_w together with the quantities $M/(\theta v_c^2)$ and $M/(\theta v_w^2)$. Again, because of its higher accuracy, we use v_w for analysis. Figure 11 shows ln v vs M. The plot shows a clear deviation from linearity by displaying downward curvature. A linear regression slope gives $(1/2)u_c = 0.125 \pm 0.006$. If u_c is assumed to have the value 1, then $v \sim \exp 0.125$ M which does not agree with Hui et al.'s asymptotics in that the prefactor for M has about one quarter the expected value. On the other hand, if u_c is treated as a parameter we find u_c has the apparent value of $\simeq 0.25$ for the range of M used in Figure 11 and conclude that Figure 11 confirms the asymptotic form in so far as the plot can be considered linear.

These results show that the asymptotic forms predicted by Hui et al. (1987b) for the "slow front" case give a very good representation of the θ dependence of v but only a fair representation of the M dependence of v. However, regarding the latter conclusion, we point out that the quantity $M/(\theta v_w^2)$ was less than 0.22 over the range of conditions explored (Table 4), instead of satisfying $M/\theta v_w^2 \ge 1$ as required by Hui's asymptotic analysis. Also, we have not employed the restrictive assumption, Eq. 13. Either of these might explain the deviations from the expected asymptotic law seen in Figure 11.

Nonetheless the numerical data clearly supports the view that the formula $v \sim \theta^{-1/2}$ is not sensitive to the details of how the diffusion coefficient increases with concentration or how

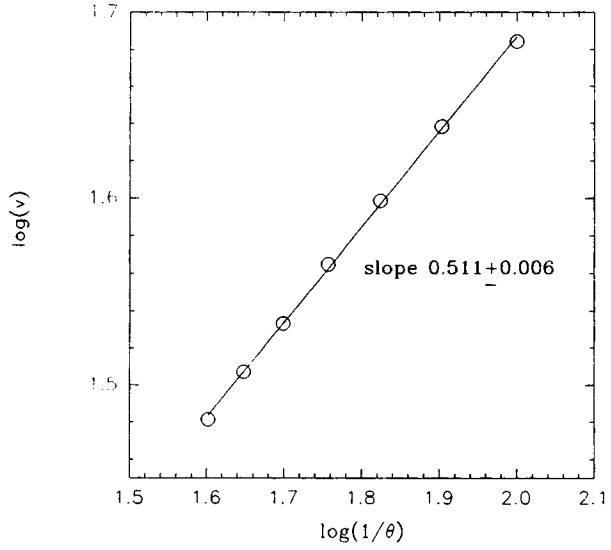

Figure 10. Logarithmic plot of the Case II front velocity, v, as a function of the inverse of θ.

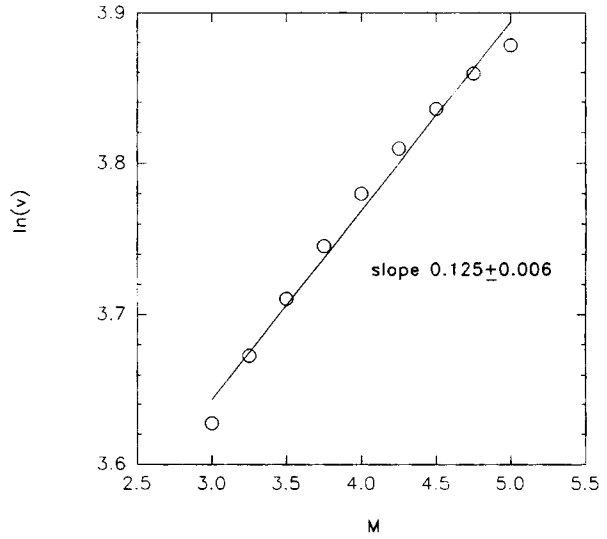

Figure 11. Semilog plot of the Case II front velocity, v, vs. M.

viscosity function decays with concentration, but only depends on these properties being strongly nonlinear. In this sense $v \sim \theta^{-1/2}$ appears to be a robust law. Unfortunately, verification of the asymptotic formulas for the M dependence of v for "fast fronts" (Eq. B1) is not accessible by our numerical scheme.

Summary and Conclusions

We showed that Thomas and Windle's model is a small Deborah number limit of the more general thermodynamic theory of Durning and Tabor (1986). We studied the model numerically for integral sorption in a dry film.

Our numerical scheme used collocation on Hermite cubics and a stiff ODE integrator (LSODI). With parameters typical of a system showing Case II, the numerical solutions clearly simulate the process correctly. Numerical values of the induction times s_i measured from the surface kinetics verified Thomas and Windle's (1982) numerics for s_i and the analytical asymptotic formula (Eq. 12) by Hui et al. (1987a). The simulated effects of the parameter θ on the sorption kinetics agree with physical intuition: For large θ (thin films) sorption is controlled by the surface swelling, on the other hand, for small θ (thick films) the sorption becomes diffusion-controlled.

The study shows that strong nonlinearities in both diffusivity and viscosity are essential for the prediction of Case II transport from a TW type model. Also, we demonstrated that the formula $v \sim \theta^{-1/2}$ by Hui et al. (1987b) was correct despite the fact that for our results we did not adopt the same severe simplifying assumptions.

In carrying out these calculations, we found that the code can run easily, and fairly fast, on 386 PC computers with a math coprocessor, so it can be used as a practical tool for routine data analysis. In the future, to improve the code's ability to solve cases with more severe nonlinearities one might try a method of generating ODEs different from collocation. For example, using Galerkin's method might reduce the chance of instability in the case that a sharp front develops in the concentration profiles, since Galerkin's technique solves the "weak form" of the original field equation (Davis, 1984; Carrier and Pearson, 1976). Also, one might choose a more advanced IVP solver appropriate for an ODE system in the form of $g(y, \dot{y}, t) = 0$. A possible technique is discussed by Petzold (1983).

Acknowledgment

We thank Dr. G. Prokopakis and Dr. A. Hindmarsh for helpful discussions and acknowledge the National Science Foundation (grant #CTS-89-19665) for financial support. We also thank a referee for pointing out an error in the original manuscript regarding our interpretation of Thomas and Windle's numerical results.

Notation

a = fluid activity; shift function for time-concentration superposition (Appendix A)
A = matrix in implicit form of coupled system of first-order ODEs (Eq. 18)
c = fluid mass concentration per unit polymer volume
c_c = critical concentration for the divergence of D in analysis by Hui et al. (1987b) (Eq. 13)
c_f = value of c at Case II front in analysis by Hui et al. (1987b) (Eq. 14)
c_e = value of c at equilibrium
d = D/D_o (Appendix A)
d' = D'/D_o (Appendix A)
D = polymer material diffusion coefficient
D' = coefficient of memory term in diffusion flux (Eq. 3)
D_{12} = binary mutual diffusion coefficient
De = diffusion Deborah number (Appendix A)
D_o = $D(c=0)$
f = dimensionless fluid chemical potential at equilibrium, relative to pure liquid
f = inhomogeneous term in coupled system of first-order ODEs
g = G/G_o
G = instantaneous shear modulus of polymer/fluid mixture
G_o = $G(c=0)$
G = inhomogeneous term in coupled system of first-order ODEs (Eq. 18)
h_j = jth sub interval size; $\zeta_{j+1} - \zeta_j$
h_n = time step size
I = dimensionless memory integral in flux expression (Appendix A)
j = dimensionless fluid flux
j_1^2 = fluid mass flux relative to polymer
k = phenomenological constant in $D(c)$
k_i = constants in linear multistep integration formula (Eq. 17)
K = kc_e
m = phenomenological constant in $\eta(c)$
m_1 = dimensionless constant related to mixture viscosity (Appendix A)
M = mc_e
n = exponent in power law expression for initial weight uptake kinetics
nx = number of subintervals
p = dimensionless, stretched age
$\hat{p}$ = dimensionless age
q = max(k_1, k_2), defines accuracy of linear multistep integration formula
r = residual function for field equation
R = gas constant; local residual based on the trial function $\tilde{u}$
s = dimensionless time
s_i = dimensionless induction time
S = region of absolute stability for $\dot{y} = \lambda y$ in the Re-Im plane of $h\lambda$ for linear multistep integration methods
t = time
t_i = initial thickness of polymer film
t_n = time after n integration steps
T = absolute temperature
u = dimensionless fluid concentration (c/c_e)
u_c = dimensionless critical concentration for the divergence of D
u_f = dimensionless fluid concentration at Case II front
u_s = dimensionless fluid concentration at film surface
v = dimensionless Case II front velocity
v_c = dimensionless front velocity determined by tracking the Case II front
v_w = dimensionless front velocity determined from weight uptake kinetics
$\hat{v}_i$ = partial specific volume of component i
$\tilde{v}_i$ = partial molar volume of component i
v_i = velocity of component i
V = Case II front velocity
W = dimensionless fluid mass uptake
y = column vector of unknowns
y_n = numerical estimate of y at t_n

Greek letters

α_j = coefficients in linear multistep integration formula (Eq. 17)
α_i^j = unknown time dependent functions in trial solution (Eq. 15)
$\boldsymbol{\alpha}$ = vector of unknown α_i^j
β = dimensionless function in asymptotic solution for v (Eq. 14)
β_j = coefficients in linear multistep integration formula (Eq. 17)
δ = Dirac function
ζ = dimensionless distance ($\zeta = \xi/t_i$)
ζ_i = position of interelement boundary

ζ_{ij}^c = collocation points
η = mixture shear viscosity
η_0 = $\eta(c=0)$
θ = parameter in dimensionless form of TW model
λ_i = eigenvalue of the Jacobian of f
Λ = dimensionless position of Case II front
μ_i = chemical potential of component i
ν_2 = value function
ξ = polymer material coordinate along the diffusion direction
Π = dimensionless nonequilibrium contribution to fluid chemical potential implied by Eq. 6
ρ = mixture mass density
ρ_i = mass density of component i
ρ_{1e} = mass density of fluid at equilibrium
σ_i = slope function
τ = shear relaxation time
τ_i = time constants for a system of first-order ODEs
φ_r = dimensionless shear relaxation modulus of mixture
ψ = decaying part of (normalized) memory function for mixture (Appendix A)
ω = mass of fluid absorbed per unit area
ω_i = mass fraction of component i

Literature Cited

Alfrey, T., E. F. Gurnee, and W. G. Lloyd, "Diffusion in Glassy Polymers," *J. Polym. Sci. C*, **12**, 249 (1966).

Astarita, G., and G. C. Sarti, "A Class of Mathematical Models for Sorption of Swelling Solvents in Glassy Polymers," *Polym. Eng. Sci.*, **18**, 388 (1978).

Billovits, G. F., and C. J. Durning, "Polymer Material Coordinates for Mutual Diffusion in Polymer-Penetrant Systems," *Chem. Eng. Comm.*, **82**, 21 (1989).

Burnett, D., *Finite Elements Analysis, from Concepts to Applications*, Prentice Hall, Englewood Cliffs, NJ (1987).

Carbonell, R. G., and G. C. Sarti, "Coupled Deformation and Mass-Transport Processes in Solid Polymers," *Ind. Eng. Chem. Res.*, **29**, 1194 (1990).

Carnahan, B., H. A. Luther, and J. O. Wilkes, *Applied Numerical Methods*, Wiley, New York (1975).

Carrier, G. F., and C. E. Pearson, *Partial Differential Equations, Theory and Technique*, Academic Press, New York (1976).

Crank, J., *Mathematics of Diffusion*, 2nd ed., Oxford University Press, London (1975).

Davis, M. E., *Numerical Methods & Modeling for Chemical Engineers*, Wiley, New York (1984).

Dill, E. H., "Simple Materials With Fading Memory," *Continuum Physics vII*, A. C. Eringen, ed., Academic Press, London (1975).

Durning, C. J., "Differential Sorption in Viscoelastic Fluids," *J. Polym. Sci.: Polym. Phys. Edn.*, **23**, 1831 (1985).

Durning, C. J., J. L. Spencer, and M. Tabor, "Differential Sorption and Permeation in Viscous Media," *J. Polym. Sci.: Polym. Letters Ed.*, **23**, 171 (1985).

Durning, C. J., and M. Tabor, "Mutual Diffusion in Concentrated Polymer Solutions," *Macromol.*, **19**, 2220 (1986).

Edwards, B. J., and A. N. Beris, "Unified View of Transport Phenomena Based on the Generalized Bracket Formulation," *Ind. Eng. Chem. Res.*, **30**, 873 (1991).

Ferry, J. D., *Viscoelastic Properties of Polymers*, 3rd ed., Wiley, New York (1980).

Finlayson, B., *Non-linear Analysis in Chemical Engineering*, McGraw Hill, New York (1980).

Frick, T. S., W. J. Huang, M. Tirrell, and T. P. Lodge, "Probe Diffusion in Polystyrene/Toluene Solutions," *J. Polym. Sci.: Part B: Polym. Phys.*, **28**, 2629 (1990).

Fu, T. Z., "Studies of Polymers at Solid/Liquid Interfaces Using a Quartz Crystal Microbalance," PhD Thesis, Department of Chemical Engineering & Applied Chemistry, Columbia University, New York (June, 1992).

Fujita, H., "Organic Vapors Above the Glass Transition Temperature," *Diffusion in Polymers*, J. Crank and G. S. Park, eds., Academic Press, London (1968).

Gear, G. W., *Numerical Initial Value Problems in Ordinary Differential Equations*, Prentice-Hall, Englewood Cliffs, NJ (1971).

Hindmarsh, A. C., "Linear Multistep Methods for Ordinary Differential Equations: Method Formulations, Stability, and the Methods of Nordsieck and Gear," *Lawrence Livermore National Laboratory Report UCRL-51186 Rev. 1* (Mar., 1972).

Hindmarsh, A. C., Lawrence Livermore National Laboratory, private communication (1991).

Hopfenberg, H. B., "The Effect of Film Thickness and Sample History on the Parameters Describing Transport in Glassy Polymers," *J. Memb. Sci.*, **3**, 215 (1978).

Hui, C. Y., K. C. Wu, R. C. Lasky, and E. J. Kramer, "Case II Diffusion in Polymers: I. Transient Swelling," *J. Appl. Phys.*, **61**, 5129 (1987a).

Hui, C. Y., K. C. Wu, R. C. Lasky, and E. J. Kramer, "Case II Diffusion in Polymers: II. Steady-State Front Motion," *J. Appl. Phys.*, **61**, 5137 (1987).

Jou, D., J. Camacho, and M. Grmela, "On the Non-Equilibrium Thermodynamics of Non-Fickian Diffusion," *Macromol.*, **24**, 3597 (1991).

Lustig, S. R., J. M. Caruthers, and N. A. Peppas, "Continuum Thermodynamics and Transport Theory for Polymer/Fluid Mixtures," *Chem. Eng. Sci.*, **47**, 3037 (1992).

Mehdizahdeh, S., and C. J. Durning, "Prediction of Differential Sorption Kinetics Near Tg for Benzene in Polystyrene," *AIChE J.*, **36**, 877 (1990).

Neogi, P., "Anomalous Diffusion of Vapors Through Solid Polymers. Part I. Irreversible Thermodynamics of Diffusion and Solution Processes," *AIChE J.*, **29**, 829 (1983).

Ocone, R., and G. Astarita, "Continuous and Discontinuous Models for Transport Phenomena in Polymers," *AIChE J.*, **33**, 423 (1987).

Painter, J. F., and A. C. Hindmarsh, "Livermore Solver for Ordinary Differential Equations (Implicit Form)," Lawrence Livermore National Laboratory Report L-316 (1982).

Park, G. S., "The Glassy State and Slow Process Anamolies," *Diffusion in Polymers*, J. Crank and G. S. Park, eds., Academic Press, London (1968).

Perez-Guerrero, A. N., and L. S. Garcia-Colin, "Anomalous Diffusion in Polymers: A Generalized Thermodynamics Approach," *J. Non-Equilib. Thermodyn.*, **16**, 201 (1991).

Petropoulos, J. H., "Application of the Transverse Differential Swelling Stress Model to the Interpretation of Case II Diffusion Kinetics," *J. Polym. Sci.: Polym. Phys. Edn.*, **22**, 183 (1984).

Petzold, L. R., "A Description of DASSL: A Differential-Algebraic System Solver," *Scientific Computing*, **65**, R. S. Stepleman, ed., North Holland, Amsterdam (1983).

Roseman, T. J., and S. Z. Mansdorf, *Controlled Release Delivery Systems*, Marcel Dekker, New York (1983).

Thomas, N. L., and A. H. Windle, "A Theory of Case II Diffusion," *Polymer*, **23**, 529 (1982).

Thompson, L. F., C. G. Wilson, and M. J. Bowden, *Introduction to Microlithography*, ACS Symposium Series, **219**, ACS, Washington, DC (1983).

Vrentas, J. S., C. M. Jarzebski, and J. L. Duda, "A Deborah Number for Diffusion in Polymer-Solvent Systems," *AIChE J.*, **21**, 94 (1975).

Vrentas, J. S., and J. L. Duda, "A Free Volume Interpretation of the Influence of the Glass Transition on Diffusion in Amorphous Polymers," *J. Appl. Polym. Sci.*, **22**, 2325 (1978).

Appendix A

Here we derive a nonlinear limiting form of Eq. 2 valid for small but finite values of the diffusion Deborah number, *De*. Integration by parts allows Eq. 2 to be recast in the form

$$j_{1,\xi}^2 = -D(c)\frac{\partial c}{\partial \xi} - D'(c)\frac{\partial}{\partial \xi} g(c) \int_{-\infty}^{t} \frac{\partial}{\partial t'} \varphi_r(c', t, t')[c-c']dt' \quad \text{(A1)}$$

where c means $c(\xi, t)$ and c' means $c(\xi, t')$. With the assumptions underlying Eq. 2, φ_r corresponds to the (normalized)

shear relaxation modulus of the mixture so that $\partial\varphi_r/\partial t'$ is the (normalized) memory function ([=]$1/T$).

The dependencies of φ_r and $\partial\varphi_r/\partial t'$ on c' express how the history of the liquid concentration in a polymer material element affects its memory of past deformations. For homogeneous systems concentrated in polymer, the dominant effect of changing the liquid concentration from c to c' is to rescale the relaxation times governing the decay of φ_r or $\partial\varphi_r/\partial t'$ by a "shift factor," a, depending on c and c' (Ferry, 1980). For a system dominated by a single relaxation time, this is expressed mathematically in terms of the memory function by

$$\frac{\partial}{\partial t'}\varphi_r=\frac{1}{\tau(c)a(c,c')}\psi\left(\frac{t-t'}{\tau(c)a(c,c')}\right) \tag{A2}$$

where ψ is a (dimensionless) decaying function of its argument. (In a generalization to a system with multiple relaxation mechanisms one would replace $\tau(c)$ by a sum over a distribution of relaxation times and apply the same shift factor to each.) Equation A2 asserts a simple time-concentration superposition principle analogous to the time-temperature superposition valid for thermorheologically simple materials (see, for example, Dill, 1975). In a generalization of Eq. A2 for a polymer material element with an arbitrary concentration history one replaces the argument of ψ in Eq. A2 with $\int_{t'}^{t} dt''/\tau(c)a(c,c'')$ by analogy with the effect of an arbitrary thermal history on the memory function in thermorheologically simple materials (Dill, 1975).

Now, consider the dimensionless form of Eq. A1 appropriate for an integral sorption experiment. Introducing the dimensionless quantities:

$$u=c/c_e;\quad \zeta=\xi/t_i;\quad s=tD_o/t_i^2;\quad d=D/D_o;\quad d'=D'/D_o$$

where c_e means the equilibrium value of c, and D_o is a reference value of the diffusion coefficient, leads to:

$$j=-d(u)\frac{\partial u}{\partial\zeta}-d'(u)\frac{\partial}{\partial\zeta}g(u)I(u,u') \tag{A3a}$$

where

$$I(u,u')=\int_{-\infty}^{s}\frac{1}{De(u)a(u,u')}\times\psi\left(\int_{s'}^{s}du''/De(u)a(u,u'')\right)[u-u']ds' \tag{A3b}$$

Here $j=j_{1,\xi}^2 t_i/c_eD_o$ is a dimensionless flux and $De(c)=\tau(c)D_o/t_i^2$ is the diffusion Deborah number based on the local value of the relaxation time and the reference diffusion coefficient. Also, $g(u)$, $a(u,u')$, and $De(u)$ mean the functions whose values are $g(c)$, $a(c,c')$, and $De(c)$, respectively, when $u=c/c_e$ and $u'=c'/c_e$.

Defining a stretched, dimensionless age, $p=(1/De)\int_s^{s'}ds''/a$, leads to the representation:

$$I=\int_0^{\infty}dp\psi(p)[u_{\hat{p}}(0,\zeta)-u_{\hat{p}}(Dep,\zeta)] \tag{A4}$$

where $u_{\hat{p}}(\hat{p},h)$ is the function whose value is $u(s',h)$ when $\hat{p}=\int_s^{s'}ds''/a$. For sufficiently small values of De, one can expand $u_{\hat{p}}(Dep,\zeta)$ in a Taylor series about $De=0$ to find an accurate approximation to the integral. Using a first-order approximation, the identity $(\partial u_{\hat{p}}/\partial\hat{p})_{\hat{p}=0}=-\partial u/\partial s$, and defining the dimensionless constant $m=\int_0^{\infty}dpp\psi(p)$ gives the dimensionless expression:

$$j=-d(u)\frac{\partial u}{\partial\zeta}-d'(u)\frac{\partial}{\partial\zeta}g(u)De(u)m_1\frac{\partial u}{\partial s}+O(De^2) \tag{A5}$$

as an accurate approximation to Eq. A3 in the limit of small, but finite Deborah numbers.

Appendix B

For the reader's convenience we summarize the asymptotic results of Hui et al. (1987b) on the Case II front velocity. In the "fast front" asymptotic case, where $M/(\theta v^2)\ll 1$ and $M\gg 1$, $u_f=u_c$ and

$$\beta=0.77[y\exp(-My)/|\ln(y)|]^{1/2} \tag{B1}$$

where

$$y=\frac{2}{M\ln(M)}\exp\left[-\left\{(1-\delta)\left(1-\frac{2\delta\ln(\delta)}{(1-\delta)^2}\right)^{1/2}-1\right\}\right],$$

and

$$\delta=1/[\ln(M/2)].$$

These describe the profile when the viscosity decreases very strongly with increasing fluid content.

In the "slow front" asymptotic case, where $M/(\theta v^2)\geq 1$ and M is sufficiently small, $\exp(-Mu_c)\sim O(1)$, Hui et al. found $u_f=1$ and

$$\beta=\left(\frac{|\ln(u_c)|\exp(Mu_c)}{u_c}\right)^{1/2} \tag{B2}$$

Manuscript received June 18, 1992, and revision received Oct. 26, 1992.